Thermotropic Liquid Crystallinity, Thermal Decomposition Behavior, and Aggregated Structure of Poly(propylene carbonate)/Ethyl Cellulose Blends

Zhihao Zhang, Huiliang Zhang, Qingxin Zhang, Qinghai Zhou, Hongfang Zhang, Zhishen Mo, Xiaojiang Zhao, Xianhong Wang

State Key Laboratory of Polymer Physics and Chemistry, Changchun Institute of Applied Chemistry, Chinese Academy of Sciences, Changchun 130022, People's Republic of China

Received 15 February 2005; accepted 20 June 2005
DOI 10.1002/app.23338
Published online in Wiley InterScience (www.interscience.wiley.com).

ABSTRACT: Maleic anhydride end capped poly(propylene carbonate) (PPC-MA) was blended with ethyl cellulose (EC) by casting from dichloromethane solutions. The thermotropic liquid crystallinity, thermal decomposition behavior, and aggregated structure were investigated by differential scanning calorimetry (DSC), thermogravimetry (TGA), and wide angle X-ray diffraction (WAXD). DSC exhibits thermotropic liquid crystallinity in the rich EC composition range. TGA shows that thermal decomposition temperatures were elevated upon interfusing EC into PPC-MA. WAXD corroborates that EC and PPC-MA/EC blend films cast from dilute dichloromethane solution possessed cholesteric liquid crystalline structure in the rich EC composition range, and that dilution of PPC-MA with EC increased the dimension of noncrystalline region, leading to a more ordered packed structure. © 2006 Wiley Periodicals, Inc. J Appl Polym Sci 100: 584–592, 2006

Key words: maleic anhydride end capping poly(propylene carbonate); ethyl cellulose; blends; differential scanning calorimetry; thermogravimetry

INTRODUCTION

Carbon dioxide copolymers, the copolymers of carbon dioxide and epoxides, are materials with great industrial interests because of the fixation of carbon dioxide and the biodegradability. Since Inoue et al. first synthesized carbon dioxide copolymers using organometallic compounds as catalysts under relatively mild conditions,[1] many researchers had devoted much effort to this field and made substantial advances.[2–7] We have employed a ternary rare-earth-metal catalyst with an efficiency of 85,000 g polymer per mole metal to synthesize highly alternating and high molecular weight carbon dioxide–epoxy propane copolymer, poly(propylene carbonate) (PPC).[8] The resulting PPC is completely biodegradable and pollution-free. The versatility of PPC has found utilization in one-off packaging materials, one-off dishware, board materials, etc. The major difficulties in application are noncrystalline property and lower thermal decomposition temperature.

Cellulose is one of the abundant natural polymers with renewable and biodegradable characteristics. As a derivative of cellulose, ethyl cellulose (EC) (Fig. 1) is a type of semirigid and thermoplastic liquid crystalline material, which has interesting physical and chemical properties, being quite attractive for many applications. The flexible ethyl groups confer lyotropic and thermotropic properties on EC. The glucose units provide thermal resistance and mechanical properties for EC. Although EC has been used to blend with several polymers,[9–12] there were only a few papers on thermotropic liquid crystallinity of the blends. To our knowledge, there has also been no paper on the blends of carbon dioxide copolymers and EC. Blending with EC, PPC is expected to further enhance thermal decomposition temperature and to improve aggregated structures, so as to prepare a sort of thermotropic liquid crystalline and biodegradable material with extensive application and low cast.

EC is an ether that has exhibited thermotropic liquid crystalline behavior.[13] Suto et al. described that EC showed two broad endotherms on DSC trace, one from 180 to 205°C and the second from 220 to 240°C,[14] corresponding to the solid phase–mesophase transition and the mesophase–isotropic liquid phase transition, respectively. PPC degrades easily when sub-

Correspondence to: Z. Mo (mozs@ciac.jl.cn).
Contract grant sponsor: Key Object of Chinese Academy of Sciences; contract grant number: KJCX2–206A-03.
Contract grant sponsor: Special Funds for Major State Basic Research Projects of China; contract grant number: G1999064806.
Contract grant sponsor: National Natural Science Funds of China; contract grant number: 20374051, 20274049.

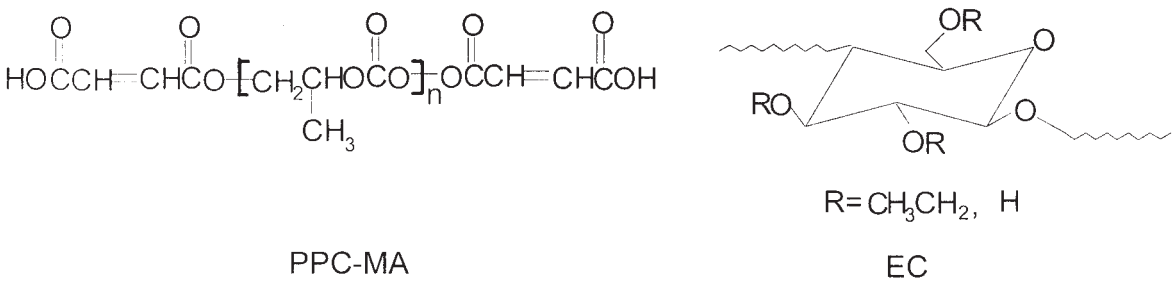

Figure 1 Chemical structures of the PPC-MA and EC.

jected to thermal treatment above 180°C.[15] To investigate the thermotropic liquid crystallinity of PPC/EC blends, the thermal stability of PPC has to be improved above all. End capping with maleic anhydride into maleic anhydride end capped PPC (PPC-MA) (Fig. 1) can improve the thermal stability of PPC.

In the present study, thermotropic liquid crystallinity, thermal decomposition behavior, and aggregated structure of PPC-MA/EC blends were investigated by differential scanning calorimetry (DSC), thermogravimetry (TGA), and wide angle X-ray diffraction (WAXD).

EXPERIMENTAL

Materials

Poly(propylene carbonate) (PPC) was synthesized by the copolymerization of carbon dioxide and epoxy propane, using a ternary rare-earth-metal catalyst.[8] The weight average molecular weight of PPC was 1,788,600.

Ethyl cellulose (EC) powder was imported from Roth Chemicals Inc. with a reported viscosity of ~0.2 Pa s and a measured molar substitution of ~2.47 by ^{1}H NMR.[16]

End capping PPC with maleic anhydride

PPC was dissolved completely in chloroform at a concentration of 10% (w/v). A stoichiometric amount of maleic anhydride was put into the mixture. After 5 h reaction, methanol was added slowly into the mixture to precipitate the crude product. The deposit was dissolved in acetone and precipitated in ethanol again. The dissolution/precipitation processes were repeated twice to completely remove the residual maleic

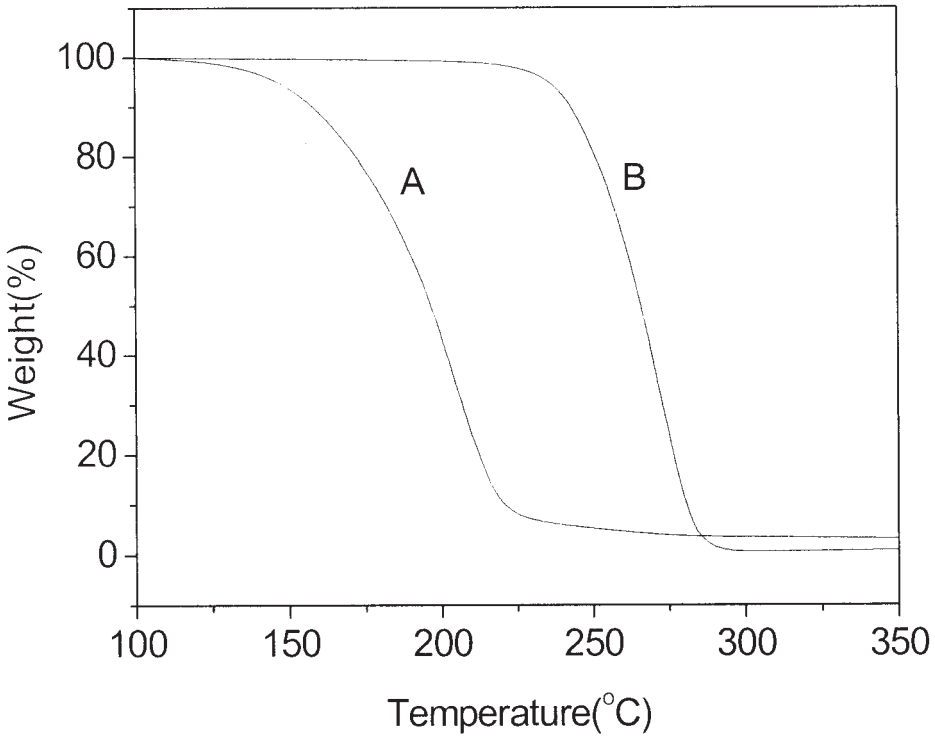

Figure 2 Thermogravimetric curves of (A) PPC and (B) PPC-MA.

TABLE I
Thermal Decomposition Temperatures for PPC and PPC-MA at a Heating Rate of 20°C/min

Thermal decomposition temperature (°C)	PPC	PPC-MA
$T_{d.5\%}$	146.0	235.4
$T_{d.95\%}$	254.4	284.0

anhydride and the other by-products from the resultant. Finally, the resultant was dissolved in acetone, precipitated in methanol, and dried under vacuum at 50°C until constant weight, before it was stored in a desiccator. The weight average molecular weight of PPC-MA was 1,104,300.

Preparation of PPC-MA/EC blends

EC powder was predried under vacuum at 75–80°C for 72 h. PPC-MA was predried under vacuum at 50°C for 24 h. Both of them were dissolved in dichloromethane (3% w/v) at 25°C, respectively. The two solutions were mixed in desired weight proportions of PPC-MA/EC. The mixed solutions were stirred and cast onto glass Petri dishes. Most solvent was allowed to evaporate at room temperature. To further remove residual solvent, all the blends were dried under vacuum at 50°C for 48 h, before they were stored in a desiccator.

Characterization

The measurements of weight average molecular weight were carried out on a Waters 410 GPC, calibrated with the monodisperse polystyrene standard, using tetrahydrofuran (THF) as an eluent at 35°C.

The thermogravimetric analyses were performed on a Perkin–Elmer TGA 7 thermal analyzer. The samples (8–9mg) were heated from 100°C at a rate of 10 and 20°C/min, respectively, in a dynamic nitrogen atmosphere.

Perkin–Elmer DSC-7 calibrated with an indium standard was used in an atmosphere of nitrogen. Typical 8–9 mg samples were heated at a rate of 20°C/min from 10 to 240°C, and then cooled rapidly to 10°C. The second heating scan was performed the same as the first. The solid phase–mesophase transition temperatures T_{CN} and the mesophase–isotropic liquid phase transition temperatures $T_{NI,}$ were taken as the peak values of endothermal curves. The transition enthalpies of blends $\Delta H_{CN,\ blend}$ at T_{CN} and $\Delta H_{NI,\ blend}$ at T_{NI} were determined from areas of endothermal curves. The glass transition temperature (T_g) was taken from the midpoint of the heat capacity change with temperature in the second heating scans.

Wide angle X-ray diffraction (WAXD) patterns were obtained at room temperature on a Rigaku D/Max 2500PC X-ray diffractometer with an 18 kW rotating-anode generator, operated at 40 kV and 100 mA, curved graphite crystal filter Cu Kα1 radiation (λ = 1.5406 Å). The mean interlayer distance d_M and mean interchain distance d_A were calculated from Bragg equation.[17] The crystallite size of mesophase region L_M and the dimension of noncrystalline region L_A were calculated from Sherrer equation,[17,18] with the shape factor k adjacent to 1.

RESULTS AND DISCUSSION

Maleic anhydride end capped PPC

The thermal degradation of PPC takes place in two steps: the chain scission, carbon dioxide is eliminated from the chain[15]; followed by chain unzipping,[3] cyclic propylene carbonate (PC) is formed.[19] End capping with maleic anhydride converted the terminal hydroxyl groups of PPC to oxygen–carbon bonds of PPC-MA and hampered chain scission and subsequent unzipping. It can be seen from Figure 2 and Table I that 5 and 95% weight loss happened to PPC at 146.0 and 254.4°C, respectively. PPC-MA showed

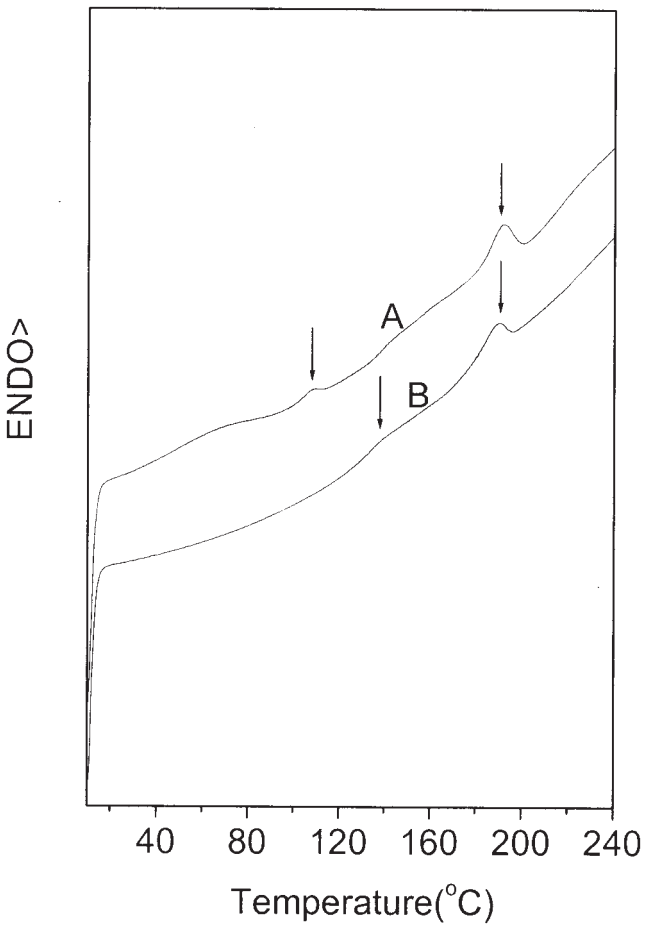

Figure 3 DSC thermograms of predried EC (A) in the first heating run and (B) in the second heating run.

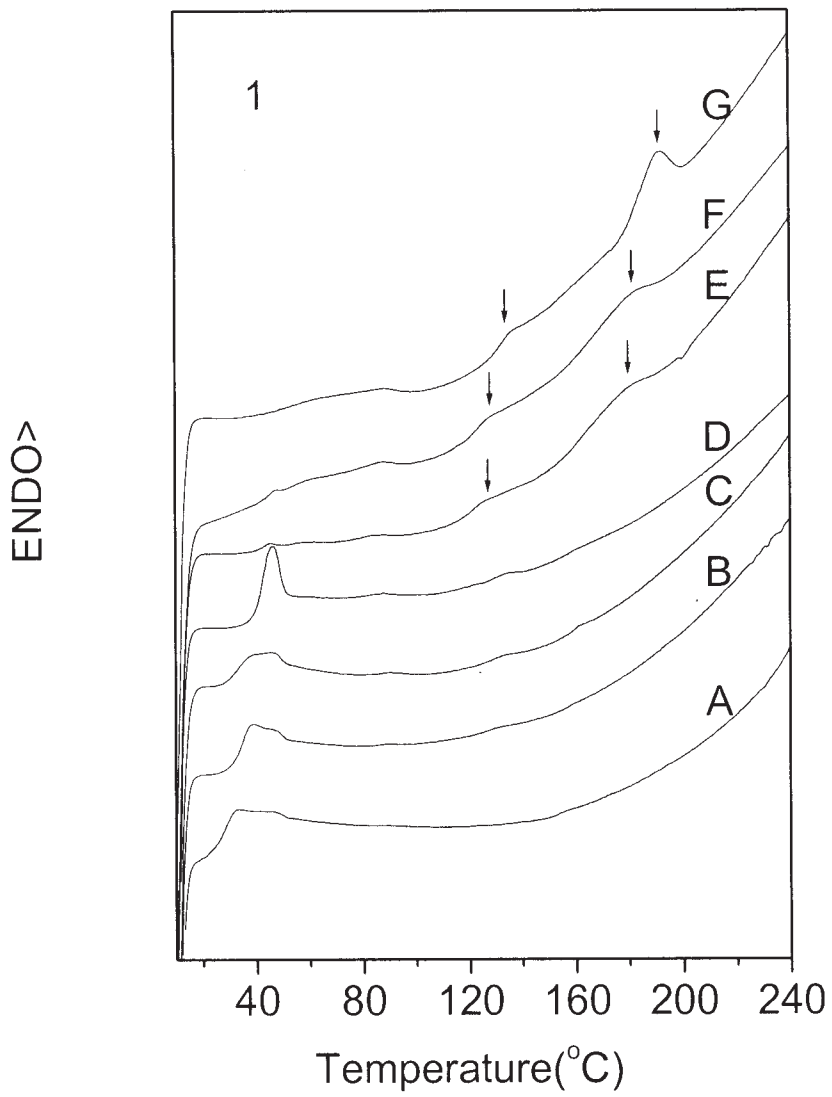

Figure 4 DSC thermograms of PPC-MA/EC blends (A) 100/0, (B) 90/10, (C) 70/30, (D) 50/50, (E) 30/70, (F) 10/90, and (G) 0/100 in the first heating runs.

around 89 and 30°C increases in decomposition temperatures of 5 and 95 wt % weight loss ($T_{d,5\%}$ and $T_{d,95\%}$), namely, 235.4 and 284.0°C. $T_{d,5\%}$ of PPC-MA approached the mesophase–isotropic liquid phase transition temperature of EC, as reported by Suto et al.[14]

Thermotropic liquid crystallinity of PPC-MA/EC blends

Figure 3 shows DSC thermograms of predried EC. The melt quenched EC had no clear glass transition, which is similar to that reported by Zhang et al.[10] This can be ascribed to supercooled liquid crystals existed below the glass transition temperature, as assumed in the discussion of poly(3-hydroxybutyrate) (PHB)/EC blends.[10] Moreover, the DSC thermograms of PPC-MA, EC, and PPC-MA/EC blends in the first and the second heating scans are exhibited in Figures 4 and 5. The solid phase–mesophase transition and the mesophase–isotropic liquid phase transition data in the two heating scans and the glass transition data in the second heating scans, as obtained from DSC, are summarized in Tables II and III. It can be seen from Figure 5 and Table III that the single glass transition temperatures T_g of the blends progressively increased with the increase of EC content in the rich PPC-MA composition range, but there were no clear glass transitions of the blends in the rich EC composition range. DSC could not illuminate the miscibility between PPC-MA and EC. We are trying to investigate the miscibility with dynamic mechanical analysis (DMA).

Chen et al. had reported that the liquid crystallinity of EC gradually perfected with increasing ethoxyl content. When ethoxyl content was 45%, one transition peak appeared on the DSC thermograms, implying

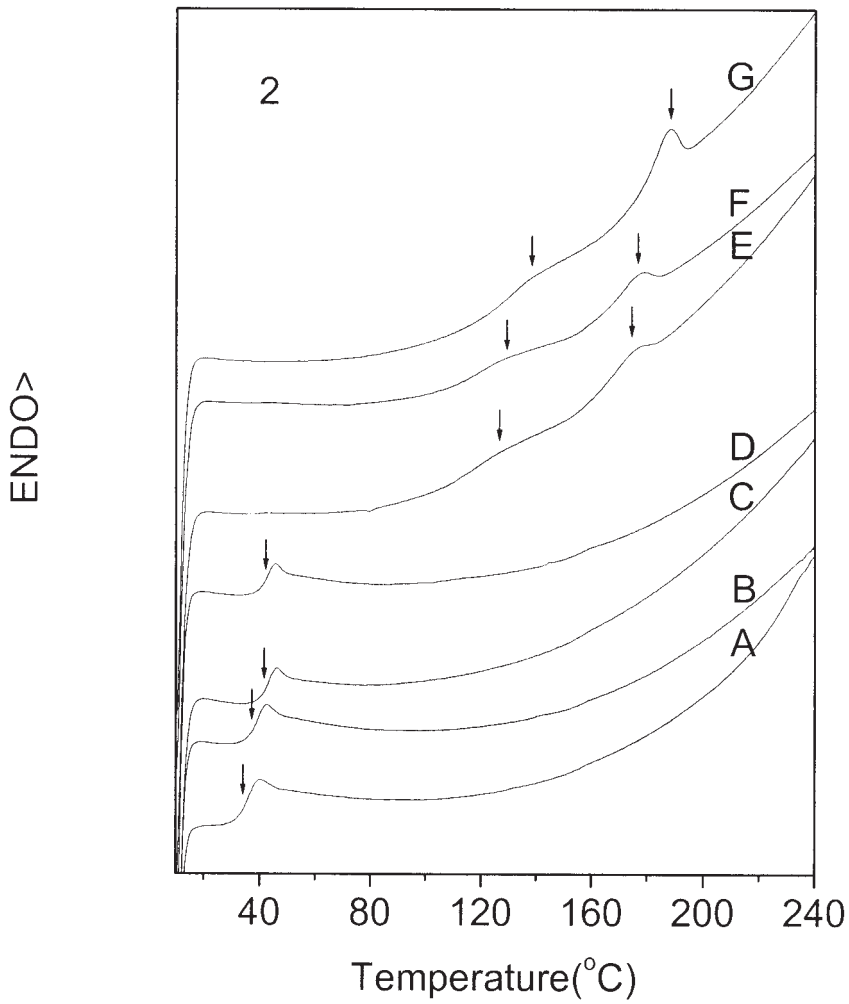

Figure 5 DSC thermograms of PPC-MA/EC blends (A) 100/0, (B) 90/10, (C) 70/30, (D) 50/50, (E) 30/70, (F) 10/90, and (G) 0/100 in the second heating runs.

the liquid crystallinity occurred. When ethoxyl content increased up to 48%, the DSC thermograms exhibited two transitions: solid phase–mesophase transition and mesophase–isotropic liquid phase transition.[20] Calculated from molar substitution, ethoxyl content of the EC used in the study was 46.6%. After the appropriate redrying procedure, EC manifested thermotropic liquid crystallinity with a solid phase–mesophase transition at ~109°C and a mesophase–isotropic liquid phase transition at ~191°C, as revealed in Figure 3, which agrees well with those obtained by Chen et al.[20] The transition temperatures were somewhat different from those obtained by Suto et al.,[14] probably arising from dissimilar ethoxyl contents,

TABLE II
Solid Phase–Mesophase Transition and Mesophase–Isotropic Liquid Phase Transition Data of PPC-MA/EC Blends in the First Heating Runs As Obtained from DSC

Composition PPC-MA/EC	Solid phase–mesophase transition			Mesophase–isotropic liquid phase transition		
	T_{CN} (°C)	$\Delta H_{CN,\ blend}$ (Jg^{-1})	$\Delta H_{CN,\ EC}$ (Jg^{-1})	T_{NL} (°C)	$\Delta H_{NL,\ blend}$ (Jg^{-1})	$\Delta H_{NL,\ EC}$ (Jg^{-1})
100/0	—	—	—	—	—	—
90/10	—	—	—	—	—	—
70/30	—	—	—	—	—	—
50/50	—	—	—	—	—	—
30/70	126.4	0.24	0.34	178.6	3.43	4.89
10/90	127.7	0.73	0.82	179.8	3.74	4.15
0/100	135.6	0.95	0.95	192.3	5.71	5.71

TABLE III
Glass Transition, Solid Phase–Mesophase Transition and Mesophase–Isotropic Liquid Phase Transition Data of PPC-MA/EC Blends in the Second Heating Runs As Obtained from DSC

Composition PPC-MA/EC	Glass transition		Solid phase–mesophase transition			Mesophase–isotropic liquid phase transition		
	T_g (°C)	ΔC_p (Jg^{-1} °C^{-1})	T_{CN} (°C)	$\Delta H_{CN,\ blend}$ (Jg^{-1})	$\Delta H_{CN,\ EC}$ (Jg^{-1})	T_{NL} (°C)	$\Delta H_{NL,\ blend}$ (Jg^{-1})	$\Delta H_{NL,\ EC}$ (Jg^{-1})
100/0	34.7	0.44	—	—	—	—	—	—
90/10	37.2	0.41	—	—	—	—	—	—
70/30	41.7	0.39	—	—	—	—	—	—
50/50	42.1	0.29	—	—	—	—	—	—
30/70	—	—	126.8	0.50	0.71	174.9	1.92	2.74
10/90	—	—	129.1	1.21	1.34	176.7	2.37	2.63
0/100	—	—	138.9	1.38	1.38	189.1	4.32	4.32

preparation conditions, measurement methods, etc. As shown in Tables II and III, the solid phase–mesophase transition temperature T_{CN}, and the mesophase–isotropic liquid phase transition temperature T_{NI} and the transition enthalpies of the blends at the transition temperatures $\Delta H_{CN,\ blend}$ and $\Delta H_{NI,\ blend}$ also increased with the increasing EC content in the rich EC composition range in the first and second heating scans, suggesting that the thermotropic liquid crystallinity increased.

Thermal decomposition behavior of PPC-MA/EC blends

The TGA traces of PPC-MA, EC, and PPC-MA/EC blends at a heating rate of 10°C/min are represented in Figure 6. The decomposition temperatures at a heating rate of 10°C/min and chart yield at 350°C obtained from TGA traces are given in Table IV. PPC-MA film achieved 5% weight loss at 235.7°C, followed by a sharp weight decrease by 95% at around 279.2°C. The chart yield at 350°C was 99.43%. On the other hand, EC possessed higher thermal stability. EC film attained to 5% weight loss at 287.1°C, and then the weight decreased gently by 95% at 427.7°C. The chart yield at 350°C was 71.63%. Compared with $T_{d,5\%}$ of pure PPC-MA, that of 90/10 PPC-MA/EC blend showed a ~9°C increase, while those of 70/30 and 50/50 PPC-MA/EC blends exhibited merely ~10 and 14°C increases, respectively; and after that, $T_{d,5\%}$ in-

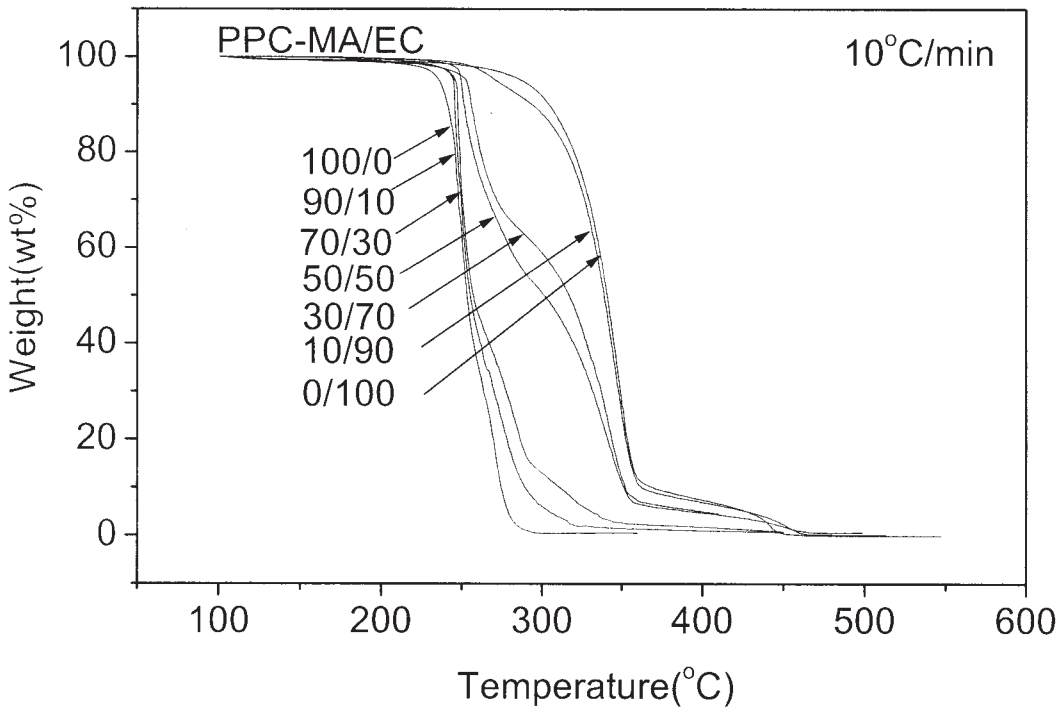

Figure 6 Thermogravimetric curves of PPC-MA/EC blends at a heating rate of 10°C/min.

TABLE IV
TGA Results of PPC-MA/EC Blends at a Heating Rate of 10°C/min

PPC-MA/EC	5% weight loss (°C)	95% weight loss (°C)	Char yield at 350°C (%)
100/0	235.7	279.2	99.43
90/10	244.4	304.9	98.47
70/30	245.8	330.6	97.37
50/50	249.3	392.4	89.20
30/70	252.7	399.6	88.11
10/90	270.9	427.5	74.73
0/100	287.1	427.7	71.63

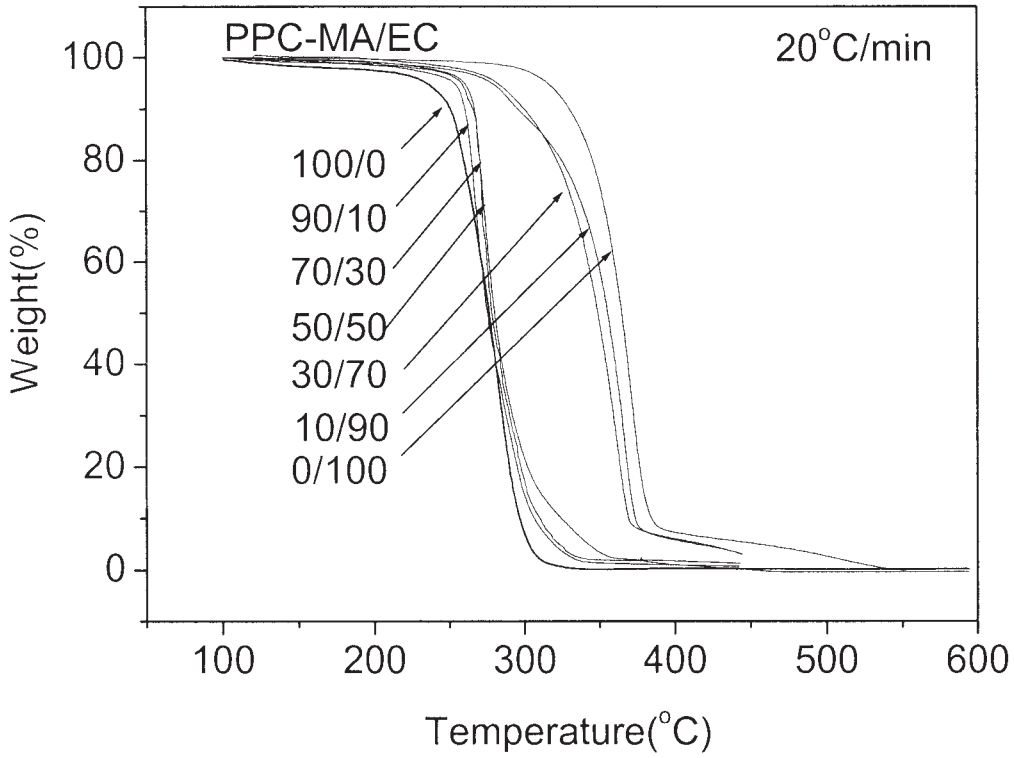

Figure 7 Thermogravimetric curves of PPC-MA/EC blends at a heating rate of 20°C/min.

creased more greatly in the rich EC composition range (Fig. 8). For the increment of $T_{d,5\%}$ with increasing weight fraction of EC W_{EC} per 10%, 90/10 PPC-MA/EC blend had the best result in the rich PPC-MA composition range, probably because the smaller amount of EC dispersed more homogeneously in the PPC-MA matrix. In the meantime, $T_{d,95\%}$ increased and chart yield at 350°C decreased with the increase of EC content. These observations prove that thermal stability of the blends was enhanced with the increase

TABLE V
TGA Results of PPC-MA/EC Blends at a Heating Rate of 20°C/min

PPC-MA/EC	5% weight loss (°C)	95% weight loss (°C)	Char yield at 400°C (%)
100/0	235.2	302.8	99.76
90/10	253.2	319.1	99.06
70/30	258.3	322.8	98.99
50/50	260.5	342.7	98.30
30/70	278.3	413.0	94.27
10/90	282.4	417.2	94.01
0/100	315.7	453.7	92.76

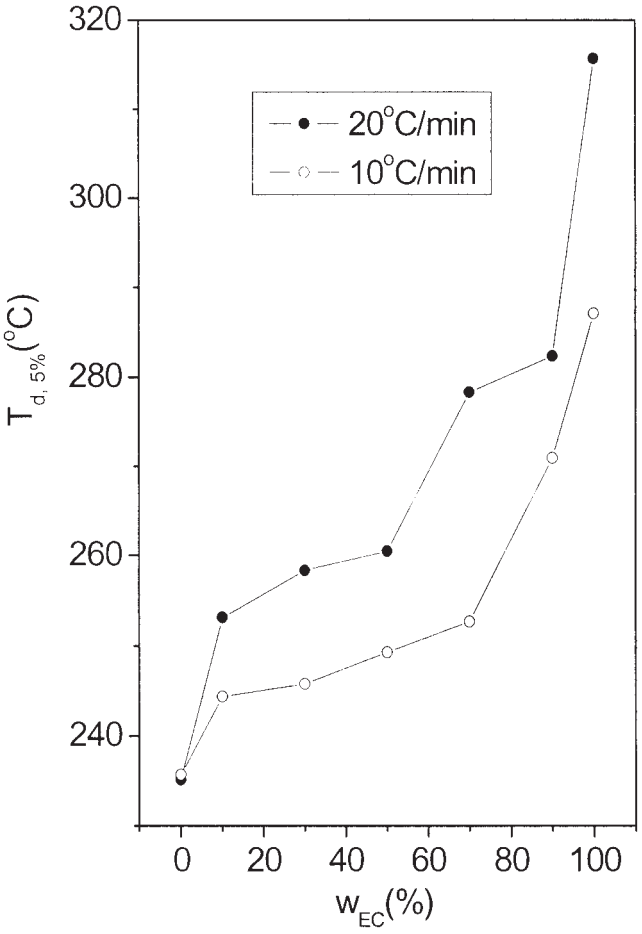

Figure 8 Decomposition temperatures of 5% weight loss temperature $T_{d,5\%}$ of PPC-MA/EC blends as a function of weight fraction of EC W_{EC}.

of EC content. The Figure 7 shows the TGA traces of PPC-MA, EC, and PPC-MA/EC blends at a heating rate of 20°C/min. Table V tabulates the decomposition temperature at a heating rate of 20°C/min and the chart yield at 400°C, obtained from TGA traces. Analogously, $T_{d,5\%}$ of 90/10 PPC-MA/EC blend was <ca18°C higher than that of pure PPC-MA, while those of 70/30 and 50/50 PPC-MA/EC blends were only 23.1 and 25.3°C higher than that of pure PPC-MA, respectively, (Fig. 8). $T_{d,95\%}$ increased and chart yield at 400°C decreased with the increase of EC content.

Aggregated structures of PPC-MA/EC blends

X-ray diffraction patterns of PPC-MA, EC, and PPC-MA/EC blends are shown in Figure 9. Pure PPC-MA showed a broad peak at 20.5°, corresponding to an interchain distance d_A of 4.34 Å. EC at room temperature exhibited two diffraction peaks at 8.7° and 19.3°, characteristic of cholesteric liquid crystallinity,[21] similar to those of hydroxyethyl cellulose acetate.[22] The low and high angle peaks corresponded to the distance between the layers of ordered polymer chains, d_M 10.86 Å, and the distance between polymer chains, d_A 4.55 Å, respectively. These observations can be explained as EC film cast from dilute dichloromethane solution. Only the EC in very thick dichloromethane solution (40–50 wt %) could form chiral nematic struc-

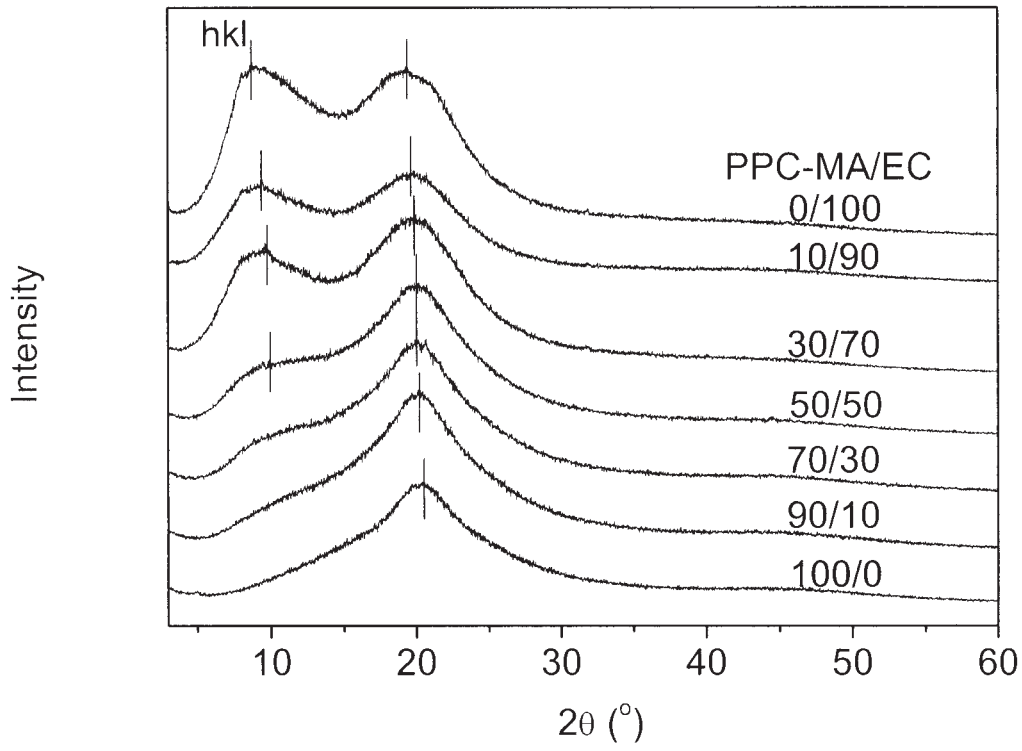

Figure 9 X-ray diffraction patterns of PPC-MA/EC blends at room temperature.

TABLE VI
WAXD Structural Parameters of PPC-MA/EC Blends

PPC-MA/EC	$2\theta_M$ (°)	d_M (Å)	L_M (Å)	$2\theta_A$ (°)	d_A (Å)	L_A (Å)
0/100	8.7	10.16	10.92	—	—	—
10/90	9.4	9.38	23.54	19.5	4.55	14.57
30/70	9.6	9.21	30.23	19.7	4.50	14.04
50/50	9.9	8.93	31.61	19.9	4.46	13.79
70/30	—	—	—	19.9	4.46	12.62
90/10	—	—	—	20.1	4.41	11.84
100/0	—	—	—	20.5	4.33	11.81

ture.[23] The X-ray diffraction pattern of EC cast film is not absolutely identical to those made by Guo and Gray[24] and Li et al.[25] because they used the EC with different viscosities and prepared the disk or film via methods different from those we did. PPC-MA/EC blends also possessed cholesteric liquid crystalline structure in the rich EC composition range. With the increase of PPC-MA content, two diffraction peaks of EC shifted somewhat toward larger Bragg angles. Accordingly, the interchain distance d_A and the interlayer distance d_M decreased, suggesting a more compact structure. Simultaneously, the low angle peak weakened whereas the high angle peak strengthened, with an increase in PPC-MA content. These phenomena are similar to those in polyvinylpyridine/EC blend membranes.[12] However, the crystallite size of mesophase region L_M increased with increasing PPC-MA content. It can be seen from Sherrer equation[17,18] that both cosin of half a scattering angle cos θ and half-width of diffraction peak β are in inverse proportion to L_M, and upon blending with PPC-MA, the declines of cos θ overwhelmed the increments of β. Dilution of PPC-MA with EC caused noncrystalline peak of PPC-MA to shift a bit towards smaller Bragg angle, and hence increase the interchain distance d_A (Table VI). Concurrently, the dimension of noncrystalline region L_A increased, namely a more ordered packing structure in the noncrystalline region, perhaps arising from the liquid crystalline EC and the hydrogen bonding between hydroxyl groups of EC and carbonyl groups of PPC-MA.

CONCLUSIONS

PPC-MA/EC blends possessed thermotropic liquid crystallinity, but no clear glass transition in the rich EC composition range. TGA shows that the thermal stability of the blends was enhanced with the increase of EC content. WAXD establishes that EC and PPC-MA/EC blend films cast from dilute dichloromethane solution possessed cholesteric liquid crystalline structure in the rich EC composition range, and that dilution of PPC-MA with EC led to a more ordered packing structure.

The other properties of PPC-MA/EC blends and the reinforcements of PPC-MA/EC blends with clay at the nanoscale level are being investigated.

References

1. Inoue, S.; Koinuma, H.; Tsuruta, T. J Polym Sci Polym Lett Ed 1969, 7, 287.
2. Kuran, W.; Gorecki, P. Makromol Chem 1983, 184, 907.
3. Dixon, D. D.; Ford, M. E.; Montell, G. J. J Polym Sci Polym Lett 1980, 18, 131.
4. Darensbourg, D. J.; Holtcamp, M. W. Macromolecules 1995, 28, 7577.
5. Super, M. S.; Beckman, E. J. Trends Polym Sci 1997, 5, 236.
6. Chen, X.; Shen, Z.; Zhang, Y. Macromolecules 1991, 24, 5305.
7. Tan, C. S.; Hsu, T. J. Macromolecules 1997, 30, 3147.
8. Zhao, X. J.; Liu, B. Y.; Wang, X. H.; Zhao, D. Q.; Wang, F. S. Chinese Pat. 98,125,654 (1998).
9. Guo, R.; Dong, Y.; Qiu, X. Chin J Cell Sci Tech 1998, 6, 17.
10. Zhang, L.; Deng, X.; Huang, Z. Polymer 1997, 38, 5379.
11. Li, X.-G. Kresse, I.; Springer, J.; Nissen, J.; Yang, Y.-L. Polymer 2001, 42, 6859.
12. Finelli, L.; Scandola, M.; Sadocco, P. Macromol Chem Phys 1998, 199, 695.
13. Farell, G. W.; Fellers, J. F. J Polym Eng 1986, 6, 263.
14. Suto, S.; White, J. L.; Fellers, J. F. Rheol Acta 1982, 21, 62.
15. Inoue, S.; Tsuruta, T.; Takada, T.; Miyazaki, N.; Kambe, M.; Takaoka, T. Appl Polym Symp 1975, 26, 257.
16. Clementt, C. J Anal Chem 1973, 45, 186.
17. Alexander, L. E. In X-Ray Diffraction Methods in Polymer Science; Wiley-Interscience: New York, 1976; Chapter 7.
18. Mo, Z.; Lee, K. B.; Moon, Y. B.; Kobayashi, M.; Heeger, A. J.; Wudl, F. Macromolecules 1972 1985, 18.
19. Inoue, S. CHEMTECH 1976, 6, 588.
20. Chen, J. N.; Huang, Y. F.; Yan, S. Q. J Appl Polym Sci 1992, 45, 2153.
21. Huang, Y. J Appl Polym Sci 1994, 1979, 51.
22. Dubini, B. Mariani, P.; Ponzi Bossi, M. G.; Rustichelli, F. Mol Cryst Liq Cryst 1983, 99, 319.
23. Kondo, T.; Miyamoto, T. Polymer 1998, 39, 1123.
24. Guo, J. X.; Gray, D. G. Macromolecules 2082 1989, 22.
25. Li, X.-G.; Kresse, I.; Xu, Z. K.; Springer, J. Polymer 2001, 42, 6801.